NUCLEAR ENGINEERING AND TECHNOLOGY
ISSN / eISSN 1738-5733
Publisher KOREAN NUCLEAR SOC,
NUTOPIA BLDG, 342-1 JANGDAE-DONG,
DAEJEON, SOUTH KOREA, 305-308
Volume 26-Issue 1-(2026)
https://doi.org/10.65281/708405

Digital microfluidic system and method based on double half-moon serrated electrodes

Xijun Huang[a], Xuxiong Zhong[a], Huijin Chen[b,*], Chuanpei Xu[a], Cong Hu[a], Binwen Xu[a]

[a]*Guilin University of Electronic Science and Technology school of Electronic Engineering and Automation, Guangxi Guilin 541004*

[b]*Guilin University of Electronic Science and Technology Department of Teaching Practice, Guangxi Guilin 541004*

[*]Corresponding authors ; Email: 6687900@qq.com

ABSTRACT

With the advancement and widespread adoption of digital microfluidic technology, this paper designs and fabricates a PCB-based digital microfluidic system to reduce the drive voltage and manufacturing costs of digital microfluidic chips while efficiently enhancing droplet drive capability. This system integrates with other peripherals to establish a digital microfluidic platform. A new electrode shape, a double half-moon serrated electrode, is proposed, which is capable of providing a large droplet driving force, and at the same time has the ability to freely switch the direction of droplet motion in all directions by conveniently combining and arranging them. Three kinds of double half-moon sawtooth electrodes with different scaling parameters were designed and experimentally verified to drive the droplets, and the results showed that the scaling relation A=1 was more effective, and the average velocity of the droplets in the transverse direction at 120 V was 1.18 mm/s, and the average velocity at 200 V was 2.57 mm/s, while in the longitudinal direction, the average velocity at 120 V was 0.98 mm/s and in the longitudinal direction, the average velocity at 200V is 1.88mm/s. The experimental data illustrate that the digital microfluidic electrode designed in this paper can effectively enhance the driving ability of the droplet compared with the electrodes such as rectangular electrode and sawtooth electrode.

KEYWORDS: Digital microfluidic system; Electrowetting-on-dielectric; Double half-moon serrated electrodes; Droplet manipulation; PCB-based chip

INTRODUCTION

The Digital Microfluidic Biochip (DMFB) is an example of a lab-on-a-chip that utilizes the principle of dielectric wetting [1] to automate biochemical experiments [2-4]. Digital microfluidic biochips, as shown in Fig. 1, use discrete droplets as carriers for a variety of fluidic manipulations, biochemical reactions, and biological assays on a microscopic scale. Compared with traditional microfluidic biochips based on continuous fluids, the main advantages are (1) lower cost, power consumption, and higher system integration; (2) multiple droplets can be controlled simultaneously on a large-scale chip for parallel operations, such as splitting and mixing; and (3) addressable electrodes on the chip can be reconfigured into multiple microfluidic modules.

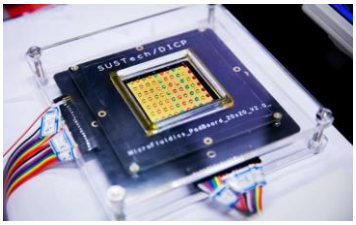

Fig. 1. Digital microfluidic chip.

Over the past decade, digital microfluidic biochips have been used for high-throughput DNA sequencing [5,6], clinical diagnostics [7,8], and protein crystallization for drug discovery [9-11]. Tom Kasputis [12]use of digital microfluidic biochips for detecting emerging pathogens and Jon Washburn [13] use of them for newborn disease screening are successful applications that demonstrate the versatility of such chips. With the integration of different types of sensors such as capacitive and optical sensors, the chip enables real-time feedback and software control, further enhancing the attractiveness of digital microfluidic platforms.

In digital microfluidic systems, there are various driving methods for manipulating droplets, such as dielectric wetting [14,15], dielectric electrophoresis [16,17], light-induced driving [18,19], surface acoustic wave [20,21] and light-driven dielectric wetting driving methods [22,23]. Nowadays, dielectric wetting (EWOD) is considered to be one of the most promising and widely used driving mechanisms. The simple structure of EWOD-based DMF chip technology, including dielectric layer, hydrophobic layer, and electrode arrays, has the advantages of high precision, simple and easy switching control of the drive system, and fast response speed, thus providing a revolutionary platform for laboratory automation and miniaturization experiments. It controls the generation and control of droplets on a microchip by applying electricity. The droplets are precisely manipulated by dielectric wetting force, and drive operations such as dispensing, moving, and splitting are performed in a programmable and addressable manner according to a preset path.

In EWOD, how to reduce the driving voltage of the droplet and at the same time improve the driving efficiency of the droplet is one of the hotspots in the research. When the voltage applied to the droplet is too high, a strong electric field is formed in the digital microfluidic chip, which is prone to cause irreversible damages to the active substances contained in the droplet [24,25]. And there are two ways to reduce the voltage: (1) the use of materials with high dielectric constants for the dielectric layer [26,27]. (2) the optimization of the electrode shape [28-30] As for the electrode shapes, the common shapes are rectangular [31], and the electrode shapes proposed to improve the droplet driving ability are serrated [32] and half-moon shape [33]. All of these electrodes are effective in improving droplet actuation, but overall, the shape of the electrodes can be further optimized to improve the performance of actuated droplets.

In this paper, starting from improving the driving efficiency of the droplets on the array electrodes and reducing the driving voltage, we design the hardware system, build the digital microfluidic platform, design different shapes of electrodes, as well as study the performance of the digital microfluidic chip for driving electrodes to reduce the driving voltage through experimental verification.

Its main innovations are as follows:

1. A double half-moon serrated electrode is proposed, which can provide both a strong droplet driving ability and a convenient combination arrangement.

2. Analyze the effect on the effective three-phase contact line of the droplet by changing the double half-moon serrated electrode with different structural parameters, and experimentally verify that the electrode shape can effectively reduce the driving voltage in order to drive the droplet.
3. Using 5CST silicone oil as the hydrophobic layer and plastic wrap as the dielectric layer ensures both usability and practicality while effectively reducing production costs.
4. Design and fabricate a PCB-based digital microfluidic platform with the advantages of simplicity, convenience, low cost and easy control.

THEORETICAL RESEARCH

Dielectric wetting fundamentals

In nature, when a droplet is placed on the surface of a solid, the droplet spreads along the contact surface with the solid under the action of surface tension, which in turn produces surface wetting [34,35]. However, since the electrically wetted droplet is in direct contact with the electrode, if a relatively large voltage applied to the electrode is given, the droplet is easily electrolyzed, and it is not possible to drive the droplet to move, and at the same time, damage may be caused to the electrode. And this phenomenon of adding a dielectric layer between the droplet and the electrode, where droplet wetting can occur, is called dielectric wetting.

The dielectric wetting process is shown in Fig. 2, where the droplets are located on top of the left and right electrodes, and the front part of the droplets is located on top of the left drive electrode, and when the left drive electrode is energized, the wettability of the surface of the microdroplet and the drive electrode with the driving voltage is changed from anaerobic to hydrophilic. The relationship between driving voltage and contact angle can be described by the Young-Lippmann equation [36] as shown in equation (1):

$$\cos\theta_v - \cos\theta_0 = \frac{\varepsilon_0 \varepsilon_r}{2\delta\gamma_{LG}} V^2$$

In Eq. (1), θ_v and θ_0 are the initial contact angle without driving voltage and the contact angle with driving voltage, respectively. ε_r is the relative permittivity of the dielectric layer, ε_0 is the vacuum permittivity, γ_{LG} is the "liquid-gas" surface tension, V is the applied voltage, and δ is the thickness of the dielectric layer. From equation (1), it can be seen that the contact angle of microdroplets decreases with the increase of driving voltage when the driving voltage increases.

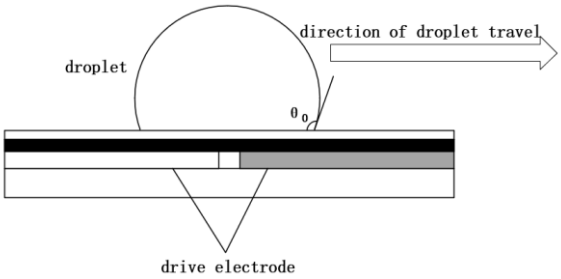

Fig. 2. Dielectric wettability.

Electrode principle analysis

The design of crescent shaped drive electrode is effective in reducing the drive voltage of the chip as compared to square and sawtooth shaped drive electrodes. In order to verify the performance of its crescent-shaped electrode, three different types of crescent-shaped electrodes were designed, and the relationship between the arc diameter and the electrode side length is:

$$A = \frac{D}{S}$$

where D is the diameter of the arc, twice the radius R, and S is the length of the electrode side. A for the three different types of crescent-shaped electrodes are 1, 1.414 and 2, respectively.

As shown in Fig. 3, the dashed circle is the droplet contact circle, and the EWOD tension generated at each point on the three-phase contact line when energization is performed is:

$$f_{er} = \frac{1}{2} CV^2$$

Calculations are made after points have been scored:

$$F_{EWOD} = f_{er} \cdot L$$

where C is the capacitance per unit area on the electric double layer, V is the applied voltage, and L is the length of the three-phase contact line. F_{EWOD} is proportional to the three-phase contact line L from Eq.4 Therefore, the larger the three-phase contact line L is, the larger its F_{EWOD} is. In comparison with the rectangular and serrated drive electrodes, the three-phase contact line of the droplet on the crescent drive electrode is relatively uniform and is the largest, in which case its droplet force is the largest and it is easier to make the droplet drive. When driving the droplets at a lower voltage than the rectangular and sawtooth drives, the crescent drive voltage is also able to drive the droplets successfully, thus realizing the purpose of reducing the drive voltage of the digital microfluidic chip. The left and right sides of the double half-moon serrated electrodes adopt this principle by symmetrically placing crescent-shaped arcs with the same parameters, which improves the droplet driving ability in both directions.

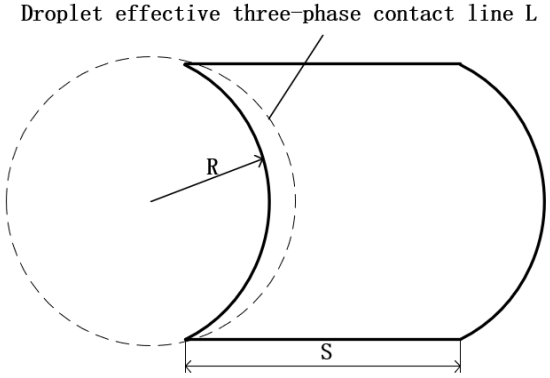

Fig. 3. Schematic diagram of half-moon electrode with droplet profile.

DMF CHIP DESIGN AND FABRICATION

DMF chip design

Common electrode shapes are rectangular [32,33], serrated [34] and crescent [35], as shown in Fig.4. Fig. 4(a) shows the rectangular electrode, which is the most basic and the first used electrode, possesses the advantages of symmetry and simple shape, but it is easy to produce the edge electric field effect, which may lead to the droplet behavior at the edge is difficult to be precisely controlled, and there are droplet deformation, uncontrolled, and so on; Fig. 4(b) shows the sawtooth electrode, which can grow the three-phase contact line compared to the matrix electrode, which can lead to enhanced electrical wetting force, giving a faster velocity of the droplets, which can be controlled using a lower voltage. At the same time, due to the overlap between the electrodes, the droplet transport can be made more

continuous and smooth. However, the disadvantages of sawtooth electrodes are also obvious; the electric field distribution is very complex and susceptible to voltage breakdown. Fig. 4(C) shows a crescent-shaped electrode, which can make the three-phase contact line longer due to the similarity of the arc of the crescent-shaped electrode to the contour of the droplet, thus providing a larger droplet driving force to drive the droplet at a faster and more uniform rate. In unidirectional movement, the droplet velocity is significantly increased compared to rectangular and sawtooth electrodes. Fig 4(D) shows a double half-moon electrode, which needs to be used in combination with a similar elliptical electrode. The double meniscus electrode adds the other side of the meniscus symmetrically to the single meniscus electrode so that the droplet drive tends to be the same on both sides. Compared with the previous single half-moon electrode, the speed of bi-directional movement of droplets is enhanced, which compensates for the lack of unidirectional droplet driving ability. Although the double half-moon electrode improves the driving ability of the droplet in the left and right directions, if it is subjected to a compositional electrode arrangement, its top and bottom directions are still rectangular electrodes, and the driving ability of the droplet and the driving voltage are not improved. In this paper, the characteristics of the double half-moon electrode and the sawtooth electrode are combined to form a double half-moon sawtooth electrode, as shown in Fig. 5. Double half-moon serrated electrodes are used in combination with ellipsoid-like electrodes in both the left and right directions to significantly enhance droplet mobility. And in the upper and lower directions, the flat rectangular edges are designed as serrated edges, the liquid droplets can move continuously and rapidly, and the electrodes can be arranged in convenient combinations with the ability to switch the direction of movement of liquid droplets freely in all directions, and they can be closely linked with the liquid separation tank, reaction tank, and waste liquid tank.

DMF chip fabrication

As shown in Fig. 6, according to Eq. (2), based on the research method, double half-moon sawtooth electrodes of 1, 1.414, and 2 were designed according to their scaling relation A.

In this paper, we use PCB design software Jialitron EDA to design and fabricate the electrodes. The package design of electrodes according to different scale relations A is carried out in the software, as shown in Fig. 6(a), as an example of designing a double half-moon sawtooth electrode with A=1. First, a circular pad with an inner diameter of 0.3mm and an outer diameter of 0.4mm is placed in the center of the canvas for linking. Next, using the document layer's lines, place four lines of 0.01mm line width and place the enclosure into a 1mm*1mm rectangle. Then, a top rectangular pad with a height of 0.7mm and a width of 0.4mm is placed in the middle of the pad. Place half-moon shaped top lines with a radius of 0.5mm symmetrically on the left and right sides of the top rectangular pads. After placing the half-moon lines, the jagged lines on the top and bottom sides of the double half-moon sawtooth shape are drawn at the starting points of the two half-moon lines, but the two sides are not positively symmetrical; instead, they are drawn with reverse symmetry because they need to be arranged in combination. Finally, using the line tool, the gap is filled, and the double half-moon sawtooth electrodes with scale relations A=1.414 and A=2 are also designed and drawn according to this method, and the final double half-moon sawtooth electrodes with scale relations A=1, 1.414, and 2 are shown in Fig. 6.

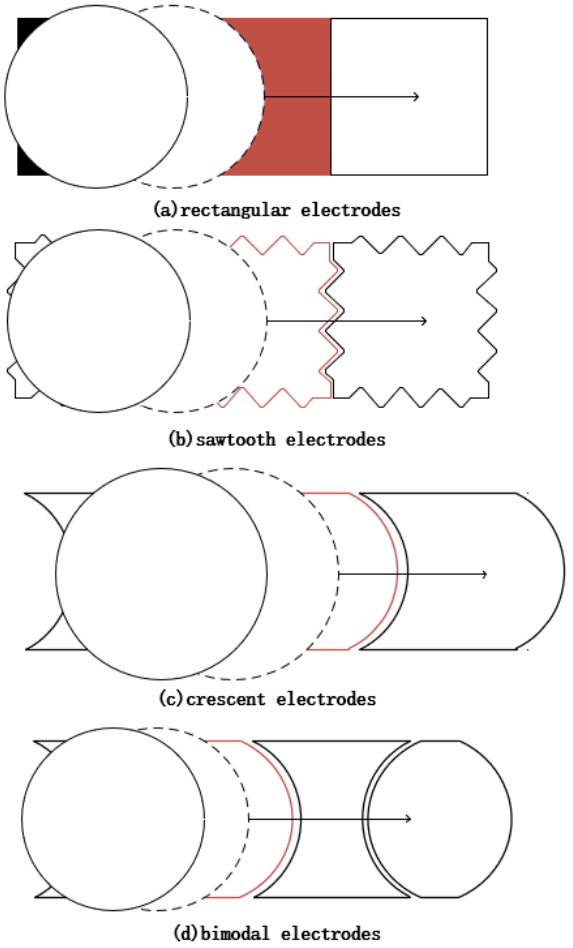

Fig. 4. Common Electrode Shapes.

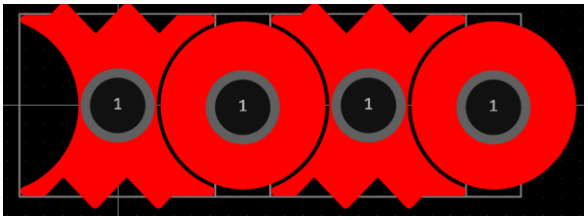

Fig. 5. Double half-moon serrated electrodes and combination electrodes.

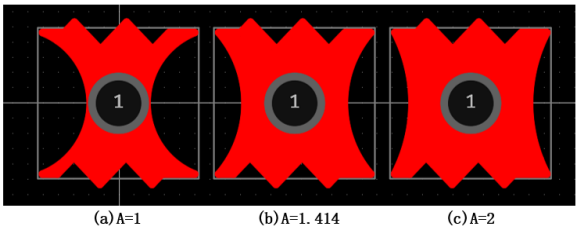

Fig. 6. Double half-moon serrated electrodes.

The ellipsoid-like electrodes used in conjunction with it are also exemplified by the proportionality relation A = 1. As shown in Fig. 7(a), first, a circular pad with an inner diameter of 0.3 mm and an outer diameter of 0.4 mm is placed in the center of the canvas for linking. Next, using the document layer's lines, place lines with a line width of 0.01mm, but unlike earlier, this needs to be placed separately. Lines of the same height as the double half-moon serrations are placed on the left and right sides, and lines of

0.298 mm length are placed on the top and bottom sides, and they are combined together. Then, a top rectangular pad with a height of 0.82mm and a width of 0.3mm is placed in the middle of the pad. Based on the two double half-moon lines on either side of the double half-moon sawtooth shape, they were plotted keeping a distance of 20 μm. Finally, using the line tool, fill in the gaps. The ellipsoid-like combination electrodes of double half-moon serrated electrodes with scale relations A=1.414 and A=2 were also designed and drawn according to this method. The ellipsoid-like combination electrodes with final scaling relations A = 1, 1.414, 2 for the double half-moon serrated electrodes are shown in Fig. 7.

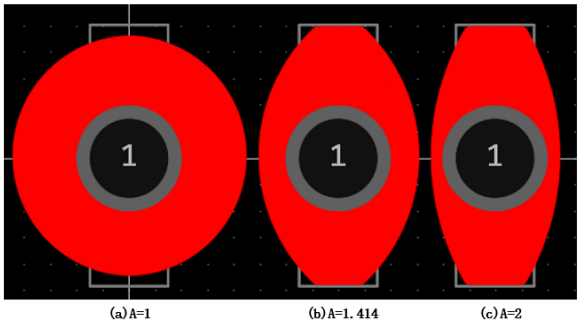

Fig. 7. Ellipsoid-like combination electrodes.

The electrodes are introduced into the circuit schematic to be arranged and combined, and the spacing between the electrodes is 20 μm, which will be fabricated into a circuit board as shown in Fig. 8. After a series of processes such as drilling, copper sinking, solder resisting, tin spraying and AVI testing in the factory, the finished products are made. The surface of the electrode plate was covered with 5 CST silicone oil as a lubricating link layer, and then a scratch-free, bubble-free, and hole-free cling film cut to the right size was placed on top as a dielectric layer. And after that, 5CST silicone oil was spin-coated as a hydrophobic layer.

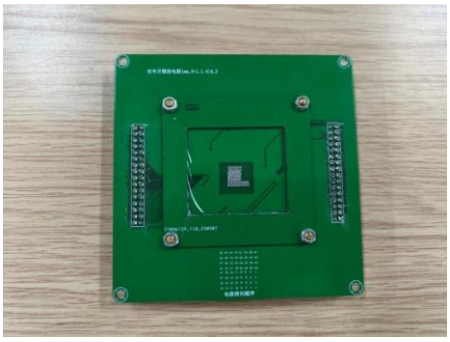

Fig. 8. Circuit board diagram.

DMF SYSTEM CONSTRUCTION

Fig. 9 shows the DMF system design. The system mainly consists of three parts: the minimum system mainly controlled by STM32F103C8T6 chip, power supply circuit and DMF chip. Send up-down-right-right control commands to the control chip through the keypad, and the microcontroller processes and executes the relevant command operations, and applies the droplet driving voltage signals to the corresponding electrodes of the DMF chip, so as to realize the droplet motion control.

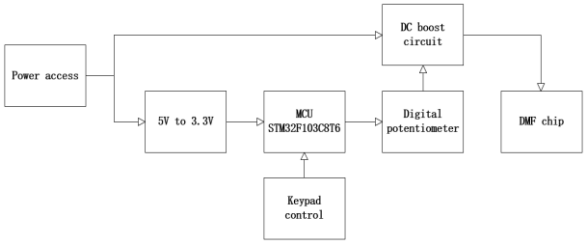

Fig. 9. DMF system flowchart.

Master chip

The main control part consists of the master chip and its peripheral circuits. The master chip model is STM32F103C8T6, a 32-bit Cortex-M3 architecture microcontroller introduced by STMicroelectronics, which is highly praised by the majority of users for its powerful performance, rich peripherals, low price, high reliability and other features. It has 37 general-purpose I/Os, 16 external interrupts, 4 timers, 2 hardware SPIs, 3 serial ports, and other peripherals, which meets the DMF system's requirements for the peripheral aspects of the master chip. Its 20KB SRAM and 128KB Flash also meet the storage requirements of the master control chip.

Power supply circuit

In the DMF system constructed in this paper, the power supply circuit is divided into a 5V to 3.3V circuit and a DC boost circuit because the power supply voltage of the main control chip is 3.3V and the voltage of the control electrode is over 100V.

5V to 3.3V circuit

Since the power supply voltage of the master chip in the DMF system is 3.3V, the digital circuit parts of the design are all powered by 3.3V. 5V to 3.3V circuit of the power supply chip using the U.S. AMS company introduced the 1117-3.3 chip, the regulator chip has a volume of laughs, low price and other characteristics, only 4 peripheral devices can be composed of a buck circuit, and the output current of the chip is 800mA, much higher than the digital circuit part of the maximum power consumption current.

DC Boost Circuit

For the design of the boost circuit in this system, MAX1771 is selected as the core DC-DC boost controller chip, which is mainly used to effectively convert the lower input voltage into the voltage required to drive the digital microfluidic droplet. In the boost circuit, in order to make the output voltage can be realized adjustable, according to the need, AD5272 is selected as a digital potentiometer.

The MAX1771 is a high-efficiency, wide-input-range DC-DC boost controller that integrates both pulse frequency modulation (PEN) and pulse width modulation (PWM) modes of operation. The MAX1771 contains an internal error amplifier, an oscillator, and a comparator, and these components work together to achieve a precise regulated voltage. It supports the external connection of N-channel MOSFETs as switching tubes, thus allowing the design to provide greater design flexibility by selecting the appropriate external power device based on specific power requirements.

The AD5272 chip is controlled by a resistor digital-to-analog converter (RDAC) register, which receives 10-bit or 8-bit data from the I2C serial interface and converts these digital values to the corresponding resistor tap positions to adjust the internal resistor array.

With these two chips, the power supply circuit is constructed, which not only realizes the power supply demand for the whole DMF system, but also adjusts the output voltage to the electrodes by the program according to the experimental demand.

DMF system setup

Fig.10 shows the constructed DMF system. The system is mainly composed of three parts: control system, DMF chip and power circuit system. The DMF chip is placed in the center, the power supply circuit system is placed on the left, the minimum control system with its peripheral circuits (key control) is placed on the right, and each part is linked through the row of pins and nuts. A signal is given to the microcontroller by manipulating the keys to realize the drive signal output and apply the drive voltage to the corresponding electrodes of the digital microfluidic chip. In addition, this system can observe the movement of the droplets in the chip through the cell phone camera, and can also record and measure the process of controlling the droplets.

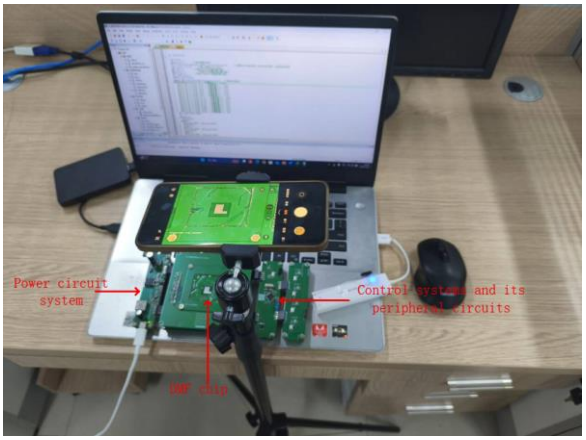

Fig. 10 DMF system.

EXPERIMENTAL VALIDATION

Before conducting the experiment, set up the pre-work, set the voltage at which the experiment is to be conducted, and commission the equipment. A certain volume of aqueous droplets was then placed on the two adjacent driving electrodes of the DMF chip using a pipette and energized to perform the experiment. The voltage of the experiment was set up before the experiment was completed and the movement of the droplets was recorded by a cell phone camera. The adjacent spacing of all three driving electrodes is 20 μm, and the voltage value is the RMS value of the voltage measured by the multimeter, Fig. 11 shows a screenshot of the experimental video of the movement of a 1 μL droplet at a certain point in time, with the droplet moving from the left to the right. Fig. 12 and Fig.13 are measured on three double half-moon serrated drive electrode structure chips at scaling relations A = 1, 1.414 and 2, respectively, where the values of the scaling relations are used to represent the different drive electrode shapes. Fig. 12 shows the relationship between the average velocity of 1 μL water droplets on three double half-moon sawtooth drive electrode chips and the driving voltage. The spacing between the electrodes and electrodes of the three drive electrodes is 20 μm, and other experimental conditions are the same, and the voltage values are the RMS values of the voltages measured by the multimeter, in which the average velocities of the

droplets were obtained from the analysis of the video of the droplet's movement. The velocity of droplet motion on the driving electrode chips of all three structures grows as the driving voltage increases, but the average velocity of the droplets on the double half-moon sawtooth electrode chip with A=1 is consistently the largest compared to the other two structures.

Experimental validation shows that when A=1, the double half-moon shaped driving electrode chip drives the droplet best, and the effect of reducing the driving voltage is most obvious. Under the same experimental conditions, the driving voltage and the average velocity of the droplet when driving the droplet movement of this type of chip outperform the other two size-proportional driving electrode structures in an important measure of the performance of the digital microfluidic chip.

In order to facilitate the upper and lower combination of the electrodes and at the same time to make the droplets move continuously and rapidly, therefore, in the upper and lower directions, the flat rectangular edges are designed as serrated edges, so that it has the ability to switch the direction of droplet movement freely in all directions, and can be closely linked with the liquid separation tank, reaction tank, and waste liquid tank. Fig. 13 shows a plot of the average speed of the sawtooth and rectangular edges versus the drive voltage. Since the same structure was used for the sawtooth edges of all three structures, one structure was randomly selected for the experiment. The experimental results show that the droplets on the sawtooth edge move faster than on the rectangular edge, regardless of the voltage.

Fig. 14 shows a combined arrangement of a double half-moon sawtooth electrode structure with scale relation A=1 and its corresponding Ellipsoid-like Combination Electrodes.

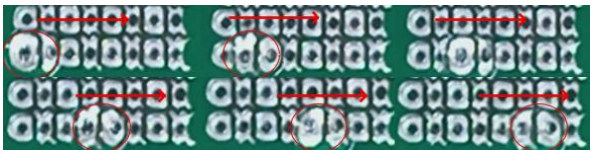

Fig. 11 Schematic diagram of droplet movement.

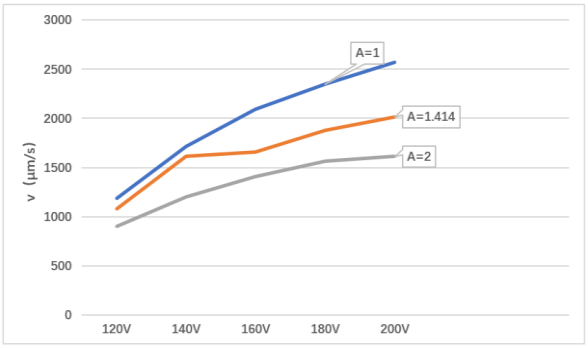

Fig. 12 Plot of average velocity of 1 μL droplet versus driving voltage.

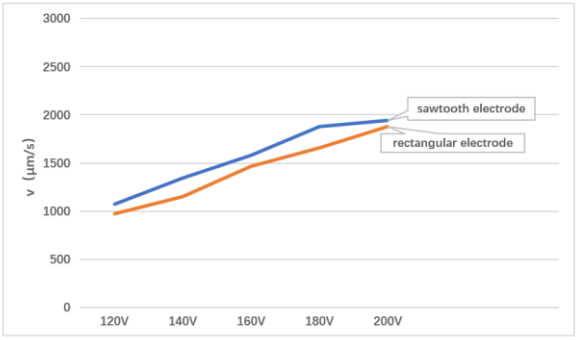

Fig. 13 Plot of Average Sawtooth and Rectangular Velocity vs. Drive Voltage.

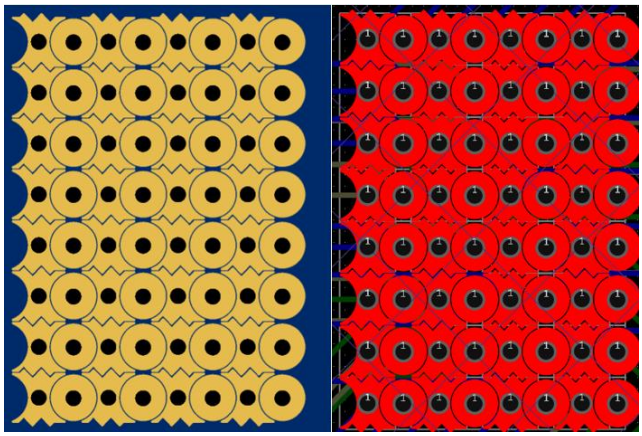

Fig. 14 Electrode combination arrangement.

COCLUSIONS

In this paper, based on the relationship between the droplet force magnitude and the droplet effective three-phase contact line magnitude, relevant research has been carried out in the design and fabrication of DMF chip and the construction of DMF system, and three kinds of double half-moon serrated electrodes with three kinds of structures have been designed, and droplet driving experiments have been carried out on the DMF chip, and the droplet driving capability of the designed three kinds of double half-moon serrated electrodes has been investigated through the experiments. The data obtained from the study show that the double half-moon sawtooth electrode with the proportionality relation A=1 drives the droplets the best, and the droplets move with the largest average velocity. This double half-moon serrated electrode is able to maintain greater overlap with the droplet at the left and right edges, which can provide a larger initial driving force, while the serrated structure at the top and bottom edges has the advantage of aligning the electrode array. After testing, the DMF system built in this paper has the characteristics of high stability, convenient combination, easy to build and easy to manipulate, which provides equipment support for this paper to reduce the manipulation voltage of digital microfluidic chip.

ACKNOWLEDGMENTS

The authors express their sincere thanks to Mingyu WU and Weiming Zeng for test PCB manufacturing as well as valuable advice during circuit debugging.

REFERENCES

1. R. B. FairCA1 (2007) Digital microfluidics: is a true lab-on-a-chip possible?, Microfluidics and Nanofluidics.3, 245-281.
2. Wang, Xingbo,Piao, Yuhao; Su, Yan; Wang, Weiqiang (2018) Driving and sorting of the fluorescent droplets on digital microfluidic platform, Microfluidics and nanofluidics.22,129.
3. M. Xie, T. Chen, X. Xin, Z. Cai, C. Dong and B. Lei (2022) Multiplex detection of foodborne pathogens by real-time loop-mediated isothermal amplification on a digital microfluidic chip, Food Control. 136, 108824.
4. X. Liu, D. Ma, H. Ye, Y. Hou, X. Bai, Y. Xing, X. Cheng, B. Lin and Y. Lu(2023) Electrowetting-based digital microfluidics: Toward a full-functional miniaturized platform for biochemical and biological applications, TrAC Trends in Analytical Chemistry. 166, 117153.

5. M. Abdelgawad (2020) Digital Microfluidics: Automating Microscale Liquid Handling, IEEE Nanotechnology Magazine. 14, 6.
6. K. Li, X. Lu, J. Liao, H. Chen, W. Lin, Y. Zhao, D. Tang, C. Li, Z. Tian, Z. Zhu, H. Jiang, J. Sun, H. Zhang and C. Yang(2024) DNA-DISK: Automated end-to-end data storage via enzymatic single-nucleotide DNA synthesis and sequencing on digital microfluidics, Proceedings of the National Academy of Sciences of the United States of America. 121, 1.
7. Sushmeeka Nair Prathaban,Nor Syafirah Zambry,Fatimah Ibrahim, Mohd Yazed Ahmad, Nurul Fauzani Jamaluddin, Tay Sun Tee (2024)Future electrodes for sepsis detection: digital microfluidic biosensors from plant waste, Microfluidics and Nanofluidics. 28, 76.
8. Hao Bai, Jie Hu, Tangyuheng Liu, Liang Wan, Cheng Dong, Dasheng Luo, Fei Li, Zhanxin Yuan, Yunmei Tang, Tianlan Chen, Shan Wang, Hongna Gou, Yongzhao Zhou, Binwu Ying, J. Huang* and W. H. (2025) A sample-to-answer digital microfluidic multiplexed PCR system for syndromic pathogen detection in respiratory tract infection, Lab on a chip. 25, 1552.
9. J. Zhai, Y. Liu, W. Ji, X. Huang, P. Wang, Y. Li, H. Li, A. H.-H. Wong, X. Zhou, P. Chen, L. Wang, N. Yang, C. Chen, H. Chen, P.-I. Mak, C.-X. Deng, R. Martins, M. Yang, T.-Y. Ho, S. Yi, H. Yao, null and Y. Jia (2024) Drug screening on digital microfluidics for cancer precision medicine, Nature Communications. 15, 4363.
10. J. Zhai, C. Li, H. Li, S. Yi, N. Yang, K. Miao, C. Deng, Y. Jia*, P.-I. Mak and R. P. Martins (2021) Cancer drug screening with an on-chip multi-drug dispenser in digital microfluidics, Lab on a chip. 21, 4749.
11. J. Shi, P. Fu and W. Zheng (2021) Lifetime improvement of digital microfluidic biochips based on the IWOA, Microelectronics Reliability. 123, 114182.
12. P.-C. Y. Tom Kasputis, Li Liu, Jeffrey Marano, James Weger-Lucarelli, Ke Du, Liwei Lin, Juhong Chen (2024) Development of a self-powered digital LAMP microfluidic chip (SP-dChip) for the detection of emerging viruses, Lab on a chip. 24, 3490 (2024).
13. D. S. M. Jon Washburn (2020) Digital Microfluidics in Newborn Screening for Mucopolysaccharidoses: A Progress Report, International journal of neonatal screening. 6, E78.
14. R. Shen, A. m. Lv, S. Yi, P. Wang, P.-I. Mak, R. P. Martins and Y. Jia (2023) Nucleic acid analysis on electrowetting-based digital microfluidics, Trends in Analytical Chemistry: TRAC. 158, 116826.
15. Xing Xu, Linfeng Cai, S. Liang, Q. Zhang, S. Lin, M. Li, Q. Yang, C. Li, Z. Han and C. Y. * (2023) Digital microfluidics for biological analysis and applications, Lab on a chip. 23, 1169.
16. T. Kim, J. Kim, J. W. Kang, S. B. Kwon and J. Hong (2022) Compact Three-Dimensional Digital Microfluidic Platforms with Programmable Contact Charge Electrophoresis Actuation, Langmuir. 38, 5759.
17. S. J. L. Seo Jun Bae, Do Jin Im (2024) Simultaneous Separating, Splitting, Collecting, and Dispensing by Droplet Pinch-Off for Droplet Cell Culture, Small (Weinheim an der Bergstrasse, Germany). 20, e2309062.
18. Y.-Y. W. Wen-Qi Ye, Dan-Ni Wang, Chun-Guang Yang, Zhang-Run Xu (2021) A digital microfluidic platform based on a near-infrared light-responsive shape-memory micropillar array, Lab on a chip. 21, 1131.
19. Y. H. Yuegan Song, Yachao Zhang, Guoqiang Li, Dawei Wang, Yi Yang, Yafeng Zhang, Yiyuan Zhang, Wulin Zhu, Jiawen Li, Dong Wu, Jiaru Chu (2022) Flexible Tri-switchable Wettability Surface for Versatile Droplet Manipulations, ACS applied materials & interfaces. 14, 37248.

20. C. C. Peiran Zhang, Xingyu Su, John Mai, Yuyang Gu, Zhenhua Tian, Haodong Zhu, Zhanwei Zhong, Hai Fu, Shujie Yang, Krishnendu Chakrabarty, Tony Jun Huang (2020) Acoustic Streaming Vortices Enable Contactless, Digital Control of Droplets, Science advances. 6, eaba0606.
21. J. Huang, X. Ren, Q. Zhou, J. Zhou and Z. Xu (2023) Flexible acoustic lens-based surface acoustic wave device for manipulation and directional transport of micro-particles, Ultrasonics. 128, 106865.
22. J. Strassner, C. Doering, E. Oliveira and H. Fouckhardt (2022) Optoelectrowetting (OEW) with push-actuation of microdroplets at small frequencies and OEW equations revisited, Sensors and Actuators A: Physical.334.
23. D. C, S. J and F. H (2021) Microdroplet Actuation via Light Line Optoelectrowetting (LL-OEW), International journal of analytical chemistry. 2021, 3402411.
24. D. E. Ying-Jia Li, Brian P Cahill, Uwe Pliquett (2019) Non-linearity and dynamics of low-voltage electrowetting and dewetting, Physical chemistry chemical physics : PCCP . 21, 18290.
25. S. Datta, P. Kumar and A. K. Das (2019) Manipulation of Droplets by Electrostatic Actuation and the Related Hydrodynamics(Review), Journal of the Indian Institute of Science. 99, 121.
26. M. Khanna, S. Roy, A. Mathur, A. K. Dubey and R. Vashisth (2021) Analysis of voltage distribution in electrowetting on Dielectric (EWOD) system, Materials Today: Proceedings. 38, 179.
27. S. Türk, A. Schug, R. Viga, A. Jupe and H. Vogt (2019) Optimization of the dielectric layer for electrowetting on dielectric, Integration, the VLSI Journal. 67, 50.
28. S. Sohail, Z. A. Jaffery and K. Biswas (2019) Study of threshold voltage for different electrode shapes in electrowetting device, Materials Research Express. 6, 046414.
29. S. Sohail, Z. A. Jaffery and K. Biswas (2019) Jigsaw electrode design for electrowetting devices(Article), Micro and Nano Letters. 14, 1046.
30. W. Wang, X. Rui, W. Sheng, Q. Wang, Q. Wang, K. Zhang, A. Riaud and J. Zhou (2020) An asymmetric electrode for directional droplet motion on digital microfluidic platforms(Article), Sensors and Actuators, B: Chemical. 324, 128763.
31. J. Guo, L. Lin, K. Zhao, Y. Song, M. Huang, Z. Zhu, L. Zhou and C. Yang (2020) Auto-affitech: an automated ligand binding affinity evaluation platform using digital microfluidics with a bidirectional magnetic separation method, Lab on a Chip - Miniaturisation for Chemistry & Biology. 20, 1577.
32. S. T. Tom Kremers, Nils Bosbach, Uwe Schnakenberg (2020) PortaDrop: A portable digital microfluidic platform providing versatile opportunities for Lab-On-A-Chip applications, PloS one. 15, e0238581.
33. Z. Wang, L. Chen and X. Bian (2020) Design of Crescent Splitting Electrodes in EWOD Device, Journal of Applied Fluid Mechanics. 13, 1437.
34. M. Torabinia, U. S. Dakarapu, P. Asgari, J. Jeon and H. Moon (2021) Electrowetting-on-dielectric (EWOD) digital microfluidic device for in-line workup in organic reactions: A critical step in the drug discovery work cycle(Article), Sensors and Actuators, B: Chemical. 330, 129252.
35. S. von der Ecken, A. A. Sklavounos and A. R. Wheeler (2021) Vertical Addressing of 1-Plane Electrodes for Digital Microfluidics, Advanced Materials Technologies. 7, 1.
36. H. J. J. Verheijen and M. W. J. Prins (1999) Reversible Electrowetting and Trapping of Charge: Model and Experiments, Langmuir. 15, 6616.